Controlling of Physicochemical Properties of Nickel-Substituted MCM-41 by Adjustment of the Synthesis Solution pH and Tetramethylammonium Silicate Concentration

Yanhui Yang, Sangyun Lim, Guoan Du, Chuan Wang, Dragos Ciuparu, Yuan Chen, and Gary L. Haller*

Department of Chemical Engineering, Yale University, New Haven, Connecticut 06520

Received: August 1, 2005; In Final Form: December 21, 2005

The effect of initial synthesis solution pH and tetramethylammonium silicate concentration in the synthesis solution on the physical and chemical properties of MCM-41 was systematically investigated using N_2 physisorption, X-ray diffraction, temperature-programmed reduction, in situ Fourier transform IR, UV−vis, and X-ray absorption spectroscopies. pH and tetramethylammonium (TMA) fraction affect the porosity of MCM-41 and the reducibility of incorporated Ni cations; higher pH and TMA concentration produced more porosity with higher stability against reduction, which is attributed to more metal ions locating in the interior of the silica walls. The control of the pore diameter of mesoporous MCM-41 at the sub-nanometer scale may be accomplished by adjusting the pH and TMA fraction. pH may be used to control the surface free silanol group density and nickel reduction degree as well, and this is useful in the design of a specific catalyst for particular reactions, such as CO methanation, which requires highly dispersed, stable metallic clusters with controllable size.

Introduction

Since the discovery of the family of siliceous mesoporous molecular sieves known as M41S, considerable attention has been paid to the investigation of the physicochemical properties of these materials.[1,2] They are prepared using a cylindrical micellar surfactant as a template, instead of individual organic molecules as with some conventional zeolites. As the best investigated member of the M41S group, MCM-41 has attracted more awareness because of its high thermal and hydrothermal stability, narrow pore size distribution with size controllable pores, and uniform shape of the pores over micrometer length scales. These properties make MCM-41 potentially applicable to the separation of proteins and selective adsorption of large molecules from effluents.[3−9] With potential catalytic applications in mind, the ability to isomorphously substitute Si by a broad range of heteroelements has been widely investigated.[10−17]

Design of an efficient catalyst for a specific reaction could optimize the catalytic activity and selectivity. To achieve this goal, in addition to control of the physical structure, chemical properties, such as the dispersion of metal ions, the state of the active component on the surface or in the framework, will be very important as well.

It has been reported that the characteristics of MCM-41 are strongly affected by the synthesis conditions, such as the mole ratio of each component in the synthesis solution, autoclaving time and temperature, pH, silica source, etc.[18] A significant improvement of the long-range order and stability of pure silica MCM-41 was reported by Ryoo and Kim through the intermediate pH adjustment of the synthesis gel.[19] In addition to the physical structure, a strong correlation of the catalytic activity for Friedel−Crafts acylation of 2-methoxynaphthalene with the pH-adjusted samples was also found by Prins' group.[20] The precise tuning of the pore size is among the many favorable properties of MCM-41. Wang and Kabe have provided a convenient way of fine-tuning the pore size of mesoporous MCM-41 by simply changing the pH.[21] Recently, highly ordered Co−MCM-41 with the metal ions dispersed on an atomic scale in the silica framework has been prepared for the synthesis of single-wall carbon nanotubes.[22] It was observed that the physical structure and the cobalt reduction patterns are very sensitive to the initial pH of the synthesis solution, which means the pH can not only control the condensation of silica but perhaps also direct the metal component to a particular location in the MCM-41 structure.

Tetramethylammonium silicate ($TMA{\cdot}SiO_2$) is an aqueous solution of an organic silica species where the silica is soluabilized by tetramethylammonium (TMA) groups. Mobil scientists used the $TMA{\cdot}SiO_2$ and HiSil as the main silica sources during the preparation of MCM-41 in their original syntheses.[2] They fixed the ratio of these two silica sources in order to control the dissolution of the colloidal silica. Recently, our group reported that the concentration of $TMA{\cdot}SiO_2$ has a dramatic influence on the synthesized V−MCM-41 catalysts in terms of physical structure and reduction behavior.[11] It is evident that there is an optimal ratio of $TMA{\cdot}SiO_2$ to colloidal silica HiSil-233 which leads to uniform mesophase structure. At higher $TMA{\cdot}SiO_2$ concentration, the vanadium incorporated MCM-41 samples have an ordered structure with a sharp capillary condensation step in the N_2 adsorption isotherm but a smaller pore diameter and a broader pore size distribution. Zero concentration of $TMA{\cdot}SiO_2$ leads to a material that has an amorphous structure; this kind of material has very little capillary condensation of liquid nitrogen and also a broad pore size distribution.

Apparently, the synthesis pH and $TMA{\cdot}SiO_2$ affect both physical and chemical properties of MCM-41 significantly, which may be used to control the physicochemical properties and perform a design of the catalysts thereafter. We are able to synthesize highly ordered Ni−MCM-41 samples with the nickel

* To whom correspondence should be addressed. E-mail: gary.haller@yale.edu.

10.1021/jp054255g CCC: $33.50
Published on Web 03/07/2006

ions dispersed on an atomic level in the silica framework. In this study, a systematic investigation of the control of physicochemical properties of nickel-substituted MCM-41 by changing the synthesis solution pH and tetramethylammonium silicate concentration was performed using temperature-programmed reduction (TPR), N_2 physisorption, X-ray diffraction (XRD), in situ Fourier transform infrared (FTIR), UV−vis, and in situ X-ray absorption (EXAFS). The effects of pH and TMA·SiO_2 concentration on the Ni−MCM-41 structure are compared to the similar Co−MCM-41 results published elsewhere.[22]

Experimental Section

Materials. Silica synthesis sources used were Cab-O-Sil from Cabot Co. and tetramethylammonium silicate (19.9% silica, Aldirch). The nickel source was $Ni(NO_3)_2{\cdot}6H_2O$ (Sigma-Aldrich Chemical Co.). The cobalt source was $CoSO_4{\cdot}7H_2O$ (Aldrich Chemical Co.). Quaternary ammonium surfactants, $C_nH_{2n+1}(CH_3)_3NBr$, were used to form the template with $n = 16$ (Sigma-Aldrich Co.) and with $n = 10$ (American Tokyo Kasei). The surfactant solutions were prepared by ion exchanging the 29 wt % $C_nH_{2n+1}(CH_3)_3NBr$ aqueous solution with equal molar exchange capacity of Amberjet-4400(OH) ion-exchange resin (Sigma Co.) by overnight batch mixing. The antifoaming agent was Antifoam A (Sigma), which is a silane polymer alkyl terminated by methoxy groups. Acetic acid (Fisher Scientific) was used for pH adjustment of the synthesis solution. In the text hereafter specific samples are designated by the initial synthesis pH value and the percentage of tetramethylammonium silicate in the total silica source (e.g., pH105 means the initial synthesis pH is 10.50; TMA50 means the tetramethylammonium silicate is 50 molar % of the total silica source).

Synthesis. The preparation process is exemplified with the sample C16 Ni−MCM-41. The surfactant solution was first prepared. The powder of cetyltrimethylammonium bromide (CTMA·Br, 20.0 g) was dissolved in deionized water (80.0 g) to make a 20.0 wt % solution. Then Amberjet 4400 OH anion-exchange resin (50 mL at the ratio of 1 mmol of surfactant/mL of resin) was added into the solution to exchange Br^- ions with OH^- ions. The ion-exchange process was performed overnight under vigorous agitation. The resulting solution was filtered and ready for use. The fumed silica Cab-O-Sil (2.5 g) was added to the tetramethylammonium silicate aqueous solution (10.4 g) and stirred vigorously for half an hour, 50.7 mL of deionized water was added to improve mixing. The nickel aqueous solution (2 wt % $Ni(NO_3)_2{\cdot}6H_2O$) or cobalt aqueous solution (2 wt % $CoSO_4{\cdot}7H_2O$) was added and stirred for another 30 min. Two drops of antifoam agent (0.2 wt % of surfactant) were added, followed by addition of the surfactant ($C_{16}H_{33}(CH_3)_3N{\cdot}OH$ 20 wt %) solution (28.7 g). The pH was adjusted to 11.5 by adding acetic acid. The final reactant molar ratios were 0.29 SiO_2 (from TMA·SiO_2):0.71 SiO_2 (from Cab-O-Sil):0.27 surfactant:0.01 Ni or Co:86 water. After additional mixing for about 120 min, this synthesis solution was poured into a polypropylene bottle and placed in an autoclave at 373 K for 6 days. After the solution was cooled to room temperature, the resulting solid was recovered by filtration, washed with deionized water, and dried under ambient conditions. The predried solid was heated at a constant rate from room temperature to 813 K over 20 h under He and held for 1 h under the same conditions, followed by calcination at 813 K for 5 h with air to remove the residual surfactant. Because the preparation process may cause some loss of Ni and Co and silica in the byproducts, the final Ni and Co content was determined by inductively coupled plasma analysis at Galbraith Laboratories, Inc. Pure siliceous MCM-41 samples were prepared with the same procedure as used for Ni−MCM-41 except without addition of nickel to the synthesis solution.

Characterization. *Nitrogen Physisorption.* Nitrogen adsorption−desorption isotherms were measured at 77 K with a static volumetric instrument Autosorb-3b (Qunatachrome). Prior to measurement, the samples were outgassed at 473 K to a residual pressure below 10^{-4} Torr. A Baratron pressure transducer (0.001−10 Torr) was used for low-pressure measurements. The pore size distribution was calculated from the desorption isotherms using the BJH method.[23] While the pore size distribution has been calculated from the desorption isothems, there would be no substantial change using the adsorption isotherms because the adsorption and desorption isotherms are ideally reversible with no hysteresis.

X-ray Diffraction (XRD). X-ray diffraction measurements were performed using a Schimadzu X-ray diffractometer (Cu Kα, $\lambda = 0.154$ nm, 40 kV, 30 mA) to check if they have the characteristic hexagonal pore structure for both the fresh Ni−MCM-41 catalysts and after reaction.

X-ray Absorption. X-ray absorption data of Ni−MCM-41 were collected at the Ni K edge (8333 eV) using a double flat Si(220) as the monochromator crystal at beam line X10C, National Synchrotron Light Source, Brookhaven National Laboratory. Approximately 200 mg of Ni−MCM-41 sample was pressed into self-supporting wafers and placed in a stainless steel cell; incident and transmitted intensities of the X-ray beam were measured by ion chambers filled with pure nitrogen. EXAFS in the transmission mode was recorded from 200 eV below to 900 eV above the Ni K edge. The spectra collected were analyzed using the UWXAFS analysis package.[24] The theoretical EXAFS functions for different nickel species (Ni and NiO) generated by the FEFF6 program were used to fit the experimental data in order to calculate the Ni−Ni and Ni−O first shell coordination numbers.[25] Details of the experimental procedure are given elsewhere.[26]

Hydrogen Temperature-Programmed Reduction (H_2 TPR). The reducibility and the stability of Ni−MCM-41 and Co−MCM-41 samples prepared were investigated by a temperature-programmed reduction using a thermal conductivity detector (TCD) of a gas chromatograph (6890 plus, Agilent). Approximately 200 mg of each sample was loaded into a quartz cell. Prior to each TPR run, the sample cell was purged by ultrazero grade air at room temperature, then the temperature was increased to 773 K at 5 K/min, soaked for 1 h at the same temperature, and cooled to room temperature. This procedure produces a clean surface, with respect to hydrocarbon contamination, before running the TPR. The gas flow was switched to 5 vol. % hydrogen in argon balance, and the baseline was monitored until stable. After baseline stabilization, the sample cell was heated at 5 K/min and held for 1 h at 1173 K to ensure complete nickel reduction. An acetone trap was installed between the sample cell and the TCD to condense water, produced by sample reduction.

DR UV−Visible Spectroscopy. Diffuse reflectance spectra were recorded in the UV−visible region on a Hewlett-Packard 8452A diode array spectrometer. The spectra were recorded in air at room temperature.

FTIR. The density of free silanol groups on the Ni−MCM-41 surface was assessed by FTIR (Nicolet). The sample was heated to 573 K for 30 min under flowing air to remove physisorbed water. The sample was cooled to room temperature in a flow of helium followed by the collection of absorption

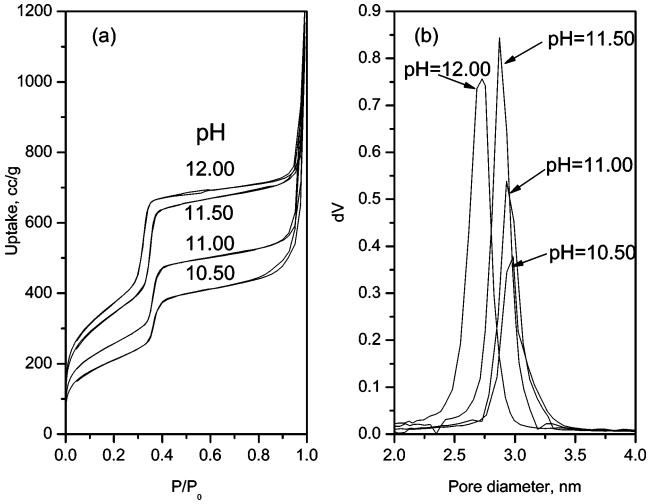

Figure 1. Nitrogen physisorption results of the C16 Ni−MCM-41 samples prepared with different pH: (a) adsorption isotherms; (b) pore size distribution.

spectrum with an observation time of 2 min. The resolution was 8 cm^{-1}.

Results and Discussion

The pH effect on the physical structure of Ni−MCM-41 was assessed by nitrogen physisorption as shown in Figure 1. All isotherms are reversible with no hysteresis; the BET C constants are large and result in a heat of adsorption in excess of 700 cal/mol in excess of the latent heat of condensation of nitrogen. It is clear that all the samples show sharp capillary condensation regardless of the pH, which indicates that all of the samples prepared have very uniform structure. There are significant changes in the isotherms and the pore volume with different initial pH of the synthesis solution. Samples prepared with higher initial pH have higher adsorption volume. Several physical properties of the Ni−MCM-41 samples are compared in Table 1. The BET surface area and mesopore volume (defined as the volume of pores having sizes below 10 nm) increase with the initial synthesis pH. These results indicate that pH controls the porosity (a secondary control, the primary being the alkyl chain length of the templating surfactant) of the Ni−MCM-41. Higher pH creates more mesopores and BET surface area; therefore, samples synthesized with higher initial pH show higher porosity. The slope of the capillary condensation of the isotherm is used as the index of structural order; larger slope suggests more uniform structure.[11] The slope of capillary condensation increases with initial synthesis pH, indicating the higher synthesis pH improves the structure. However, the slope of capillary condensation drops slightly for the sample synthesized from an initial pH of 12.0, which may be attributed to excess porosity.

The pore size distribution patterns of samples synthesized at different pH, which are calculated by the BJH method,[23] are shown in Figure 1b. All the samples prepared at pH 10.5−12.0 show narrow pore size distributions, regardless of the pH, with the full width at half-maximum (fwhm) about 0.2 nm, shown in Table 1. Compared to other samples, the sample prepared with initial pH 11.5 has the narrowest pore size distribution with the fwhm only 0.16 nm. When combined with the largest slope of capillary condensation possessed by this sample, this indicates that pH 11.5 appears to be the optimum synthesis pH for Ni−MCM-41 samples, in terms of highest structural order.

Since the variation of pH changes the OH^- concentration in the synthesis gel, as Wang and co-workers proposed, the pH of the synthesis mixture may affect the mesopores size by altering the charge matching pattern in the mixture.[21] Pore size distribution patterns clearly show that the pore diameter decreases with increasing synthesis pH and the calculated average pore diameter confirms this; see Table 1. The pore diameter changes from 2.98 to 2.73 nm with changing pH from 10.5 to 12.0. Clearly, the synthesis pH can be used for fine-tuning of the pore diameter, as well as precisely controlling the porosity of Ni−MCM-41 samples. In the synthesis mixture, OH^- groups work as the counterion. They form a charged layer of aqueous solution to balance the charges of a cationic inorganic species and an anionic surfactant. At lower pH, the thickness of the counterion layer may increase to keep the total OH^- constant in order to balance the charge, resulting in the enlargement of the pore size of the product.[21] On the other hand, pH variation may also change the electrostatic charge distribution in the mixture, affecting the interactions of headgroups in the micelle and resulting in the expansion of the micelle.[27]

X-ray diffraction was carried out for the Ni−MCM-41 samples to verify the hexagonal pore structure and calculate the pore wall thickness, although the XRD results only show local well-ordered fractions of Ni−MCM-41. All samples show highly ordered hexagonal pore structure indexed by (100), (110), (200), and (210) diffraction peaks as shown in Figure 2a, indicating that the mesostructures are well developed. Diffraction peaks shifted to lower angles with decrease of synthesis mixture pH, and the intensity of the (100) peak decreases dramatically for pH 10.5 sample, which indicates the structural order decreases with such low synthesis pH. Analysis shows that the *d* spacing and pore wall thickness increase dramatically as the synthesis pH decreases from 12.0 to 10.5, which results in more extensive silanol group condensation.

By incorporation of nickel ions in the silica framework, Ni−MCM-41 can have catalytic activity for synthesis of SWNTs and CO_2 methanation.[28] Therefore, chemical properties will be important as well as the physical properties for the purpose of designing catalysts. Temperature-programmed reduction (TPR) is a very convenient technique for studying the reduction behavior of supported oxide catalysts qualitatively. In this study, hydrogen TPR was carried out in the temperature range from 323 to 1173 K to evaluate the reduction behavior of the nickel species in Ni−MCM-41 and is used as a stability index. TPR patterns of C16−Ni−MCM-41 samples having the same nickel content but different initial synthesis pH are compared in Figure 3. Unlike the Co−MCM-41 samples, in which the synthesis pH strongly affects the Co reduction,[22] reduction of Ni−MCM-41 samples in this study did not show any correlation with the pH. All the samples have a similar temperature at the maximum reduction rate (summit of the reduction peak) regardless of the synthesis pH, shown in Figure 3a. In addition, when both the temperature at the maximum reduction rate and the temperature of reduction initiation are plotted as a function of pH, it is observed that the initial pH of the synthesis mixture has a larger effect on the initiation of reduction compared to the negligible effect on the maximum reduction rate, as shown in the Figure 3b. The Ni−MCM-41 samples with higher initial synthesis pH have higher temperature of initiation of reduction, which implies higher pH samples are more stable against reduction.

The TPR patterns of Ni^{2+} in MCM-41 showed asymmetric shapes, especially for the sample prepared with lower synthesis pH. As Lim and co-workers proposed, the radius of cobalt ions is small (∼0.07 nm) compared to the pore wall thickness of MCM-41 (∼1.0 nm); therefore, when the cobalt ions are incorporated in the framework of MCM-41 to form isolated

TABLE 1: Physical Properties of C16 Ni-MCM-41 Samples with Different pH Values

pH		pore diameter, nm	BET surface area, m^2/g	mesopore volome,[c] cm^3/g	slope of capillary condensation, a.u.	fwhm, nm	*d*-spacing, nm	pore wall thickness, nm
10.50	a	2.98	763.2	0.65	3357	0.18	4.41	1.43
	b	2.70	685.9	0.56	1419	0.36	4.12	1.42
11.00	a	2.93	931.3	0.79	4649	0.18	4.28	1.36
	b	2.77	932.7	0.81	2372	0.31	4.09	1.32
11.50	a	2.87	1245	1.12	6988	0.16	4.16	1.29
	b	2.63	1183	1.00	3784	0.23	3.89	1.26
12.00	a	2.73	1347	1.16	5812	0.21	3.91	1.18
	b	2.49	1175	0.98	3149	0.29	3.65	1.16

[a] Fresh calcined sample. [b] After complete reduction. [c] Defined as <10 nm in diameter.

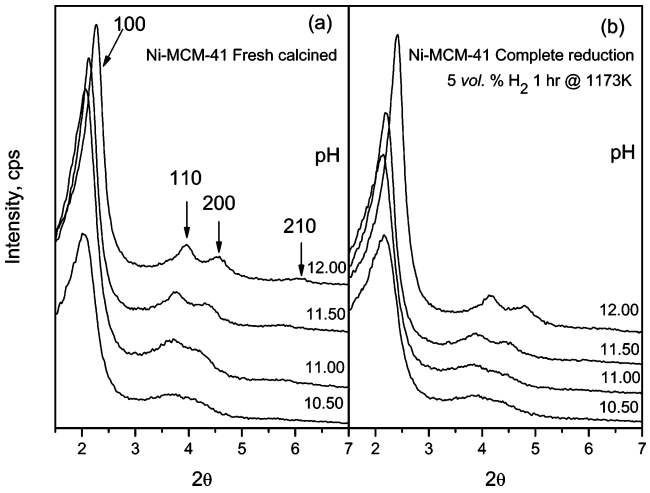

Figure 2. X-ray diffraction (XRD) patterns of the C16 Ni−MCM-41 samples with different pH: (a) fresh calcined; (b) after complete reduction.

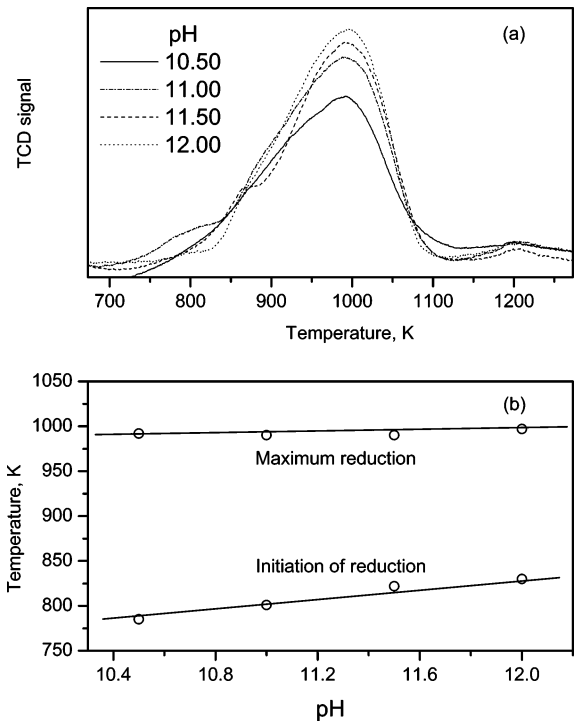

Figure 3. TPR results of C16 Ni−MCM-41 with different pH: (a) TPR profiles; (b) the temperature at the maximum reduction rate and the initiation of reduction as a function of pH.

cobalt ions, these can be distributed over several layers in the framework because the pore wall of MCM-41 consists of amorphous silica. It may be on the surface, in the interior of the silica wall, or subsurface (between these two locations); hence, the asymmetric reduction peaks might be attributed to the different location of Co ions in the framework.[22] As a next neighbor of cobalt in the periodic table of elements, nickel might have the same locating mechanism as cobalt; that is, the nickel ions might be on the surface, in the interior of the silica wall, or subsurface with respect to the pore wall.

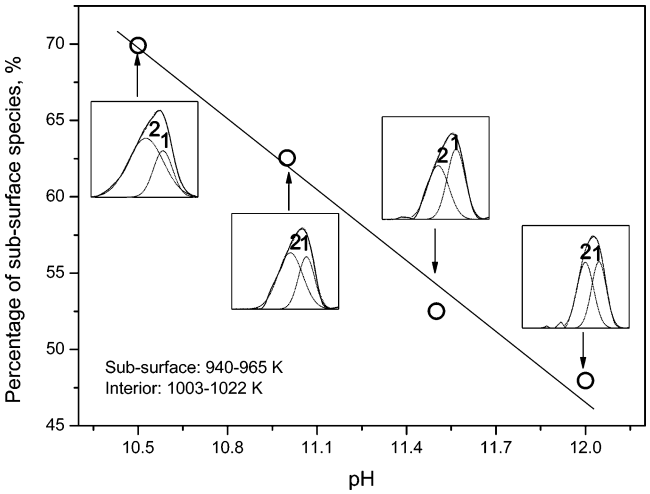

Figure 4. Deconvolution results of Ni^{2+} reduction peak of the C16 Ni−MCM-41 sample prepared from different pH. (insets) TPR profiles of Ni−MCM-41 samples prepared with different pH in the synthesis mixture and simulated TPR profiles showing the deconvolution of the peaks

The Ni−MCM-41 sample prepared hydrothermally does not show any low-temperature reduction below 800 K, which would suggest the presence of nickel oxides and nickel nitrate compounds on the silica surface. All the samples have much higher stability against reduction reflected in a higher reduction temperature relative to both Ni species, which indicates the nickel species are entirely incorporated into the silica framework, regardless of the synthesis pH. On the basis of the above discussion, we tentatively propose in this study the reduction of nickel in the framework of MCM-41 may be deconvoluted into two species, staying in either the interior or the subsurface of the silica wall of MCM-41.

Figure 4 shows the TPR profiles of Ni−MCM-41 samples prepared with different pH in the synthesis mixture and simulated TPR profiles showing the deconvolution of the peaks. The high temperature peak between 1003 and 1022 K is assigned to the reduction of nickel in the interior of silica wall (peak 1); the low temperature peak between 940 and 965 K is assigned to the reduction of a nickel species in the subsurface (peak 2), which has lower stability against reduction. Prior to running the TPR experiments, relatively more nickel ions in the interior layer were expected for lower synthesis solution pH sample

because of the thicker pore wall, which would lead to a higher temperature for the initiation of reduction. However, in this study, it is observed that the distribution of nickel ions is not associated with the pore wall thickness. It is observed that Ni−MCM-41 sample prepared with low pH is more asymmetric than high pH samples, indicating the uneven distribution of nickel in the silica wall; the low temperature shoulder suggests more nickel ions locating in the subsurface. Analysis confirms about 70% nickel ions residing in the subsurface and the remainder in the interior of silica wall. The percentage of subsurface species approaches 50% as the pH in the synthesis mixture increases to 11.5 and 12.0, which indicates the distribution of nickel ions developing more and more uniformity with respect to the silica wall. This is probably because of the better mixing due to the higher synthesis solution pH (greater silica solubility), resulting in more interaction between the nickel ions and silica source.

The distribution of Ni ions changes significantly as pH changes, pH105 has a substantial portion of subsurface nickel ions; pH115 and pH120 samples have an increased portion of nickel ions in the interior of the silica wall. Subsurface Ni ions can be reduced more easily than those in the interior as proposed by Lim and co-workers in their investigation of Co−MCM-41,[22] resulting in a shift of the initiation of reduction to higher temperature. On the other hand, nickel ions, which have such high reducibility will be reduced easily and migrate to form bigger particles, once they are pulled out of the silica wall and exposed to hydrogen.[28] This may provide rationalization for the fact that the temperature of the maximum reduction rate is the same for all the samples regardless of pH in the synthesis mixture.

Nitrogen physisorption and X-ray diffraction were used to characterize the structure of Ni−MCM-41 after temperature-programmed reduction. Highly ordered structure was conserved even under such severe conditions (1173 K in flowing hydrogen for 1 h), as shown in Figure 2b. The pore diameter of Ni−MCM-41 decreases due to the dehydroxylation, some indexes of structural order, for example, BET surface area, mesopore volume, slope of capillary condensation, and pore wall thickness decrease as well, which can be attributed to the collapse of the pore structure, as shown in Table 1.

Lim and co-workers have claimed that they are able to produce and control sub-nanometer Co clusters taking advantage of the different reduction stability created by adjustment of the initial pH of the synthesis solution.[22] In this study, we demonstrate further that we may be able to control the reduction stability of nickel ions as well by adjusting the pH. X-ray absorption experiments of the Ni−MCM-41 samples with different initial synthesis solution pH values were carried out to calculate the cluster size produced from each sample. As shown in Table 2, the average first shell Ni−O coordination number is around 5 for the fresh calcined hydrated samples. It will drop to around 4 once the samples are dehydrated,[28] which indicates the local tetrahedral coordination of nickel ions in silica framework. The in situ reduction was performed under flowing pure hydrogen at 873 K for 30 min, the average first shell Ni−Ni coordination number decreases monotonically from 6 to 4 with increasing pH from 10.5 to 12.0, and the average first shell Ni−O coordination number increases monotonically from 0.6 to 2. In fact, the calculation of coordination number is highly dependent on the normalization of edge absorption. If the Ni had some average coordination environment with Ni and oxygen absorption, analyzing the windowed Ni−O and Ni−Ni peaks together as a linear combination from the Ni would appear to give a useful answer. However, in our experiments, the coordination environment is closer to a physical mixture of small Ni metal clusters and Ni oxide clusters, due to the incomplete reduction of nickel. It would seem that it would be more appropriate to analyze separately the windowed Ni−O and Ni−Ni peaks in R-space, to somehow normalize the Ni−Ni to the fraction of metal in the sample and use this as a quantitative measure of metal cluster size. However, there is no analysis software that can solve this problem at the present time because the reduction degree cannot be determined prior to the analysis. In this work, we tentatively use the variation of Ni−O coordination number of fresh and reduced sample as the index of the reduction degree. Table 2 shows that fewer nickel cations were reduced with increase of pH of the initial synthesis solution, which is consistent with the hydrogen TPR results, and more nickel ions locate in the interior of the silica framework of the sample prepared with higher pH in the synthesis mixture, which has higher stability against reduction. On the other hand, these extremely small metal clusters with several atoms could be anchored to unreduced Ni ions in the framework producing high stability and high dispersion on the surface, as proposed by Lim and co-workers,[22] which makes the Ni−MCM-41 a promising catalyst for the reactions requiring careful control of prereduction, such as the synthesis of single-wall carbon nanotubes, CO methanation and CO_2 methanation, etc. After normalized by the reduction degree, it is clearly observed in Table 2 that the first shell Ni−Ni coordination number is constant regardless of the synthesis solution pH; this is probably because of the higher reducibility of nickel. All nickel ions were reduced at the same temperature regardless of the pH; therefore, once the nickel has been reduced, they will be pulled out and migrate with the same rate on the surface and coalesce together to form the larger clusters with about the same size eventually.

TABLE 2: Average First Shell Ni−O and Ni−Ni Coordination Number of C16 Ni-MCM-41 with Different pH Values

		coordination number			
		pH = 10.50	pH = 11.00	pH = 11.50	pH = 12.00
fresh calcined[a]	Ni−Ni				
	Ni−O	5.23	5.50	5.02	5.34
reduced[b]	Ni−Ni	5.94	5.88	5.65	4.26
	Ni−O	0.61	0.72	0.85	2.02
normalization	reduction degree	88%	87%	83%	62%
	Ni−Ni	6.75	6.76	6.80	6.87

[a] Hydrated samples. [b] Samples were reduced in pure H_2 at 873 K for 30 min.

As described elsewhere, some of the variables that influence the preparation of MCM-41 interact with other synthesis variables.[11] To isolate the pH effect from other synthesis parameters (e.g., incorporation of nickel ions), siliceous MCM-41 samples with different initial pH were prepared and compared to Ni−MCM-41, as shown in Figure 5. Clearly, all the siliceous MCM-41 and Ni−MCM-41 samples when prepared with the same initial pH are nearly identical in terms of pore diameter, slope of capillary condensation, mesopore volume, and the BET surface area, which indicates that the incorporation of nickel ions does not affect the pH effect in this study. All the effects of pH on the physical properties of Ni−MCM-41 discussed previously are pure pH effects on the silica MCM-41. It may be that the pH affects silica MCM-41 formation significantly and both Ni and Co are in such minority concentration that their

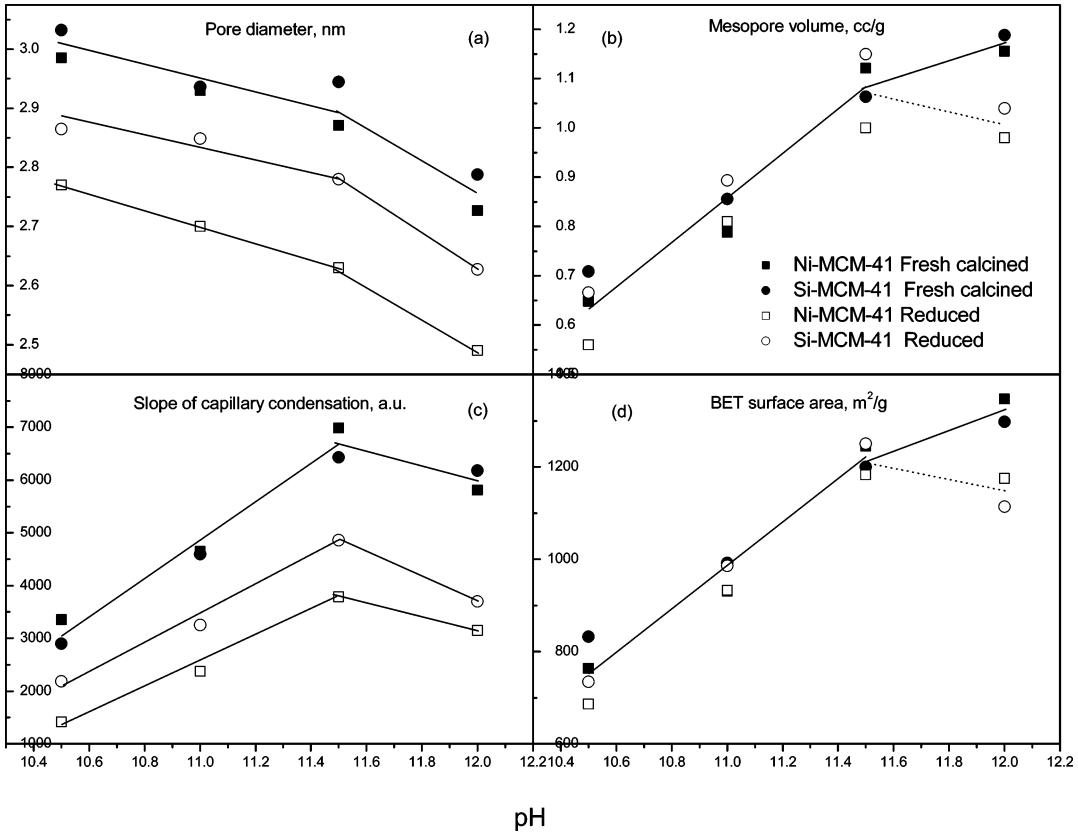

Figure 5. Comparison of physical properties of C16 Si−MCM-41 and C16 Ni−MCM-41 samples with different pH: (a) pore diameter; (b) mesopore volume; (c) slope of capillary condensation; (d) BET surface area.

effects are trivial compared to pH. However, the Si−MCM-41 and Ni−MCM-41 show different stability against reduction once the hydrogen temperature programmed reduction was carried out. The pore diameter and the slope of the capillary condensation of both the Si−MCM-41 and Ni−MCM-41 decreases after the TPR experiments as shown in parts a and c of Figure 5, which indicates a decrease in the structural order of MCM-41. Ni−MCM-41 samples have lower stability compared to Si−MCM-41. This may be attributed to the complete reduction of nickel ions; all the nickel ions are reduced and pulled out of the silica framework resulting in a decrease in structural order due to the defects. On the other hand, the porosity, indicated by the mesopore volume and the BET surface area, does not change significantly after hydrogen reduction except for the pH120 sample, which may be attributed to the excess porosity, as shown in parts b and d of Figure 5.

During the synthesis process, two silica sources, tetramethylammonium silicate (TMA·SiO_2) and Cab-O-Sil, were used. TMA·SiO_2 is an aqueous solution of an organic silica species where the silica is soluabilized by tetramethylammonium groups (TMA). The concentration of TMA has a dramatic influence on the final structure of synthesized Ni−MCM-41 samples, as shown in Figure 6. At higher TMA concentration, the Ni−MCM-41 samples have the same kind of ordered structure but with a smaller pore diameter and a broader pore size distribution. Low concentrations of TMA lead to a material that has an amorphous structure; this kind of material has very little capillary condensation of liquid nitrogen, larger pore diameter, and also a broad pore size distribution. We can see from Figure 6 that there is an optimal ratio of TMA·SiO_2 to Cab-O-Sil which leads to uniform mesophase structure.

The TMA has an almost identical effect on the isotherms of Co−MCM-41 as it does on the Ni−MCM-41 synthesis (not

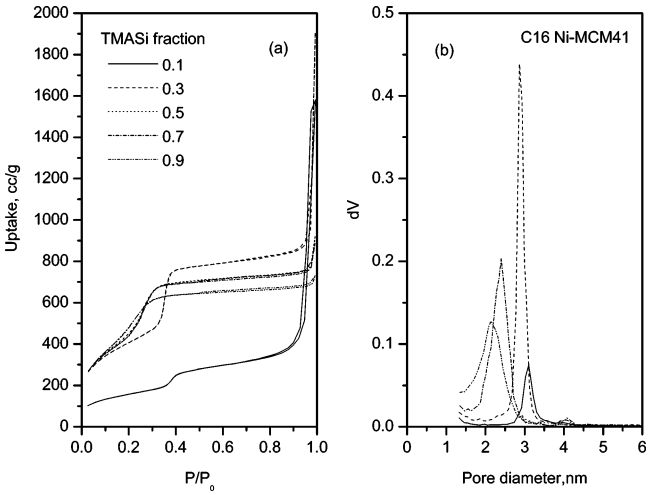

Figure 6. Nitrogen physisorption results of the C16 Ni−MCM-41 samples with different tetramethylammonium silicate concentrations: (a) adsorption isotherms; (b) pore size distributions.

shown here). X-ray diffraction was also used to assess the physical properties for both Ni−MCM-41 and Co−MCM-41. The physical properties of Ni−MCM-41 and Co−MCM-41 with different TMA·SiO_2 concentrations are compared in Table 3. It can be observed that the BET surface area and mesopore volume increase with increasing TMA concentration, which indicates that the higher TMA concentration yields higher porosity of MCM-41. Higher TMA concentration is desirable for the formation of porous materials. TMA is a soluble organic silica and will enhance the solubility of the silica source and reduce the possibility of agglomeration, which may promote the building of the physical structure of MCM-41; moreover, the TMA source may accelerate the condensation of silica

TABLE 3: Comparison of Physical Properties of C16 Ni-MCM-41 and C16 Co-MCM-41 Samples with Different TMA Concentration

TMASi fraction	BET surface area, m^2/g		mesopore volume, cm^3/g		pore diameter, nm		*d*-spacing, nm		pore wall thickness, nm		slope of capillary condensation, a.u.	
X-MCM-41[a]	Ni	Co	Ni	Co	Ni	Co	Ni	Co	Ni	Co	Ni	Co
0.10	571	557	0.36	0.29	3.10	3.02	4.90	4.93	1.81	1.91	1495	1390
0.30	1478	1452	1.29	1.34	2.87	2.85	4.08	4.09	1.21	1.24	7331	8079
0.50	1604	1435	1.16	1.13	2.94	2.94	3.51	3.17	1.11	1.01	2775	1410
0.70	1569	1605	1.26	1.02	2.40	1.96	3.40	3.18	1.19	1.08	2535	1167
0.90	1711	1561	1.17	1.24	2.14	2.30	3.37	3.34	1.23	1.04	1654	1141

[a] X = Ni or Co.

because of its higher solubility. On the other hand, the TMA source likely also has a kinetic effect, i.e., is more reactive than inorganic oligomers and may even create a kinetically driven "virtual pressure" that results in a smaller pore. Therefore, the pore diameter, *d* spacing, and the pore wall thickness decrease with higher TMA group concentration. The same phenomenon was observed for vanadium-substituted MCM-41 reported elsewhere.[11] Hence, the TMA source concentration is another convenient way to control the structure and porosity of MCM-41 and tune the pore diameter precisely, which is very important to the design of catalysts. When the physical properties of MCM-41 with different TMA source concentrations are compared in Table 3, it is observed that Ni−MCM-41 and Co−MCM-41 behave similarly with the change of TMA source concentration from 0.10 to 0.90, which confirms that all the synthesis parameters will affect physical properties of Ni−MCM-41 and Co−MCM-41 in the same way. Note also that change in pore wall thickness as a function of TMA source concentration is similar for Ni- and Co−MCM-41, but one will see that the two metals respond differently with regard to reducibility. This suggests that TMA effect on the wall thickness is not the dominant effect of TMA on reducibility.

Local environment of nickel in the silica framework has been investigated by X-ray absorption elsewhere,[28] and it is confirmed by UV−vis spectroscopy in this study. Figure 7 shows the UV−vis patterns of Ni−MCM-41 samples with different TMA group concentrations, comparing with the reference compounds, octahedral coordinated NiO, and tetrahedral coordinated $NiAl_2O_4$, which was synthesized according to ref 28 and confirmed by X-ray diffraction. Different geometries of nickel(II) have quite different spectra in the ultraviolet and visible portions of the spectrum; these absorptions are due to d−d transitions. Octahedral nickel typically has three absorptions, 340, 410, and 710 nm, according to the NiO absorption spectrum. Tetrahedral nickel has a similar spectrum but shifted to lower energies when compared to an octahedral nickel; a strong absorption near 650 nm is typical of tetrahedral nickel(II) as seen in the spectrum of $NiAl_2O_4$. It is clearly observed that all the samples prepared, regardless of the TMA fraction, have a strong absorption around 650 nm which demonstrates the tetrahedral coordination of nickel in the silica framework. All the spectra of Ni−MCM-41 show weak absorption at 340 and 410 nm in addition to the absorption at 650 nm, which are assigned to the octahedral coordinated nickel. This suggests that the nickel in the silica framework is either in a distorted tetrahedral coordination or a mixture of tetrahedral and octahedral coordination, which is consistent with the X-ray absorption results. The absorption intensity around 650 nm decreases, the 410 nm absorption increases, with an increase in the TMA fraction, which indicates that the TMA group promotes the transformation of tetrahedrally coordinated nickel to octahedral nickel. The reason for this transformation is still unclear.

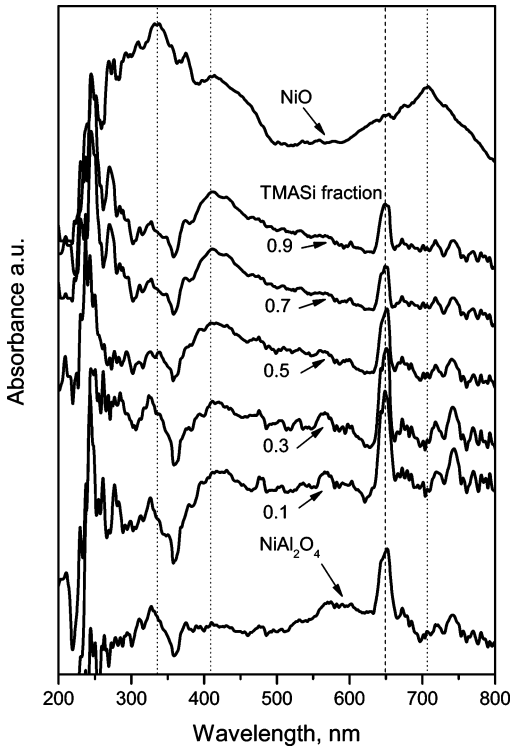

Figure 7. UV−vis absorption patterns of C16 Ni−MCM-41 samples with different TMA group concentrations, compared with references.

The reducibility of metal has been related to the activity and the selectivity of catalysts. Understanding of the reduction behavior is, therefore, essential for the design of the catalysts. Both hydrogen TPR and in situ XANES-TPR results show that Co−MCM-41 and Ni−MCM-41 have high stability against hydrogen reduction; the maximum reduction temperature is over 900 K. However, unlike Co−MCM-41, in which the radius of curvature of pores, metal loading, and pH in initial synthesis solution strongly affect the Co reduction, reduction of Ni−MCM-41 samples did not show any correlation with any of these synthesis parameters. All of the Ni−MCM-41 samples have the same temperature at the maximum reduction rate regardless the pore size, pH, or metal loading. Figure 8 shows the comparison of reduction patterns of Co−MCM-41 and Ni−MCM-41 as a function of tetramethylammonium silicate fraction, which is another very crucial factor during the synthesis. Apparently, the reducibility of Co−MCM-41 has a strong correlation with the TMA fraction. Higher TMA concentration leads to both higher temperature of the maximum reduction rate and the initiation of reduction, which result in a higher stability of reduction. On the other hand, even though the TMA fraction does not affect the temperature of Ni−MCM-41 at the maximum reduction rate significantly due to the thermodynamics of reduction, it controls the temperature of the initiation of reduction, which could be

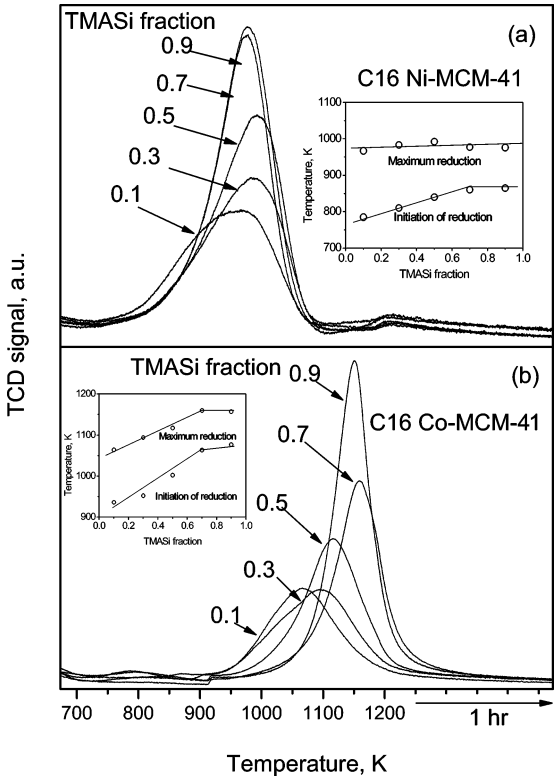

Figure 8. Comparison of TPR patterns of C16 Ni−MCM-41 and C16 Co−MCM-41 as a function of TMA group fraction.

applied to control the reducibility of Ni−MCM-41. On Comparison of the cobalt- and nickel-substituted MCM-41, the reduction patterns of Co−MCM-41 are more symmetric than those of the Ni−MCM-41. Deconvolution results show that unlike the distribution of nickel ions in the framework, which is located in both the subsurface and interior of silica wall (higher TMA fraction leads to higher portion of interior nickel ions, which makes the reduction more difficult), the cobalt ions locate either in the subsurface (low TMA fraction) or in the interior (high TMA fraction) with respect to the silica wall, which makes the reduction profile more symmetric.

The measured density of surface free silanol groups reflects the polymerization of silica in the synthesis solution, which might be used to explain the contribution of TMA group during the synthesis. The surface silanol groups of Ni−MCM-41 with different initial TMA fraction were measured by FTIR in the diffuse reflectance mode as shown in Figure 9. The Kubelka−Munk function of absorbance was calculated, and the intensity of the free silanol group at wavenumber 3745 cm^{-1} of each sample, normalized by the BET surface area, is compared in the inset of Figure 9. As expected, the intensity of free silanol groups decreases monotonically with the initial TMA fraction in the synthesis solution. As the soluble silicate increases, the silica particles become more negatively charged and increasingly repel each other; therefore, they do not collide, so that particle growth continues without aggregation, which perhaps results in a maximum of siloxane (Si−O−Si) bonds and a minimum of uncondensed Si−OH groups.

High TMA fraction of total silica can reduce the pore diameter dramatically, which might make the presence of micropores in MCM-41 possible. As described elsewhere,[10] the presence of micropores in Co−MCM-41 templates is undesirable because the pores can be interconnected by micropores resulting in the formation of nonuniform carbon nanotubes. Comparative plots with the physisorption results were carried out to determine

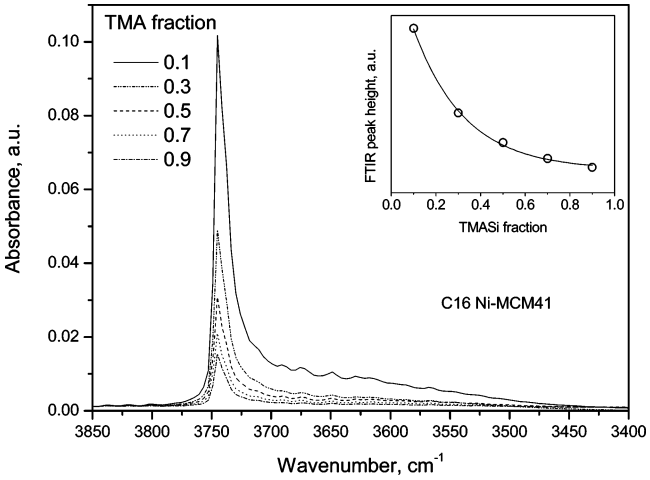

Figure 9. FTIR results of the fresh calcined C16 Ni−MCM-41 samples with different TMA group fraction. (inset) Intensities of Si−OH at 3745 cm^{-1} plotted with TMA fraction of each sample.

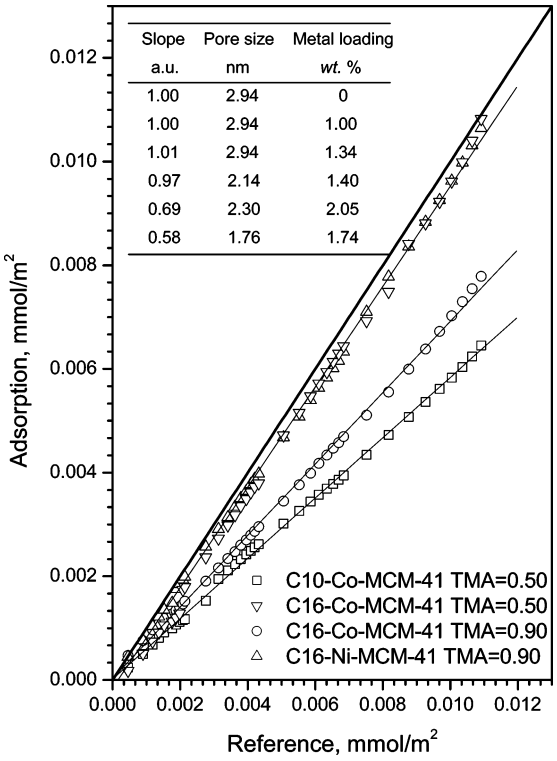

Figure 10. Comparative plot of Ni−MCM-41 and Co−MCM-41 samples with different TMA group fractions.

whether micropores are present in the MCM-41 samples with high TMA group fraction, and the results are shown in Figure 10. The number of moles of adsorbate (nitrogen) per unit area of each sample was compared with that of a reference sample containing no micropores. The extrapolated linear portions of the plots recorded for samples with different TMA fraction pass through the origin, confirming the absence of micropores. Therefore, the TMA concentration may be used to control the pore diameter, avoiding the introduction of micropores.

Conclusions

Precise control of the physical and chemical properties of metal ions incorporated in the MCM-41 matrix can be achieved by the adjustment of pH and the tetramethylammonium silicate concentration in the initial synthesis solution. Adjusting pH and

TMA fraction affects the porosity of MCM-41, surface free silanol group density, and the metal ion distribution in the silica framework. Higher pH and TMA concentrations produce more porosity with higher stability against reduction, which is attributed to more Ni or Co ions locating in the interior of the silica wall. We can fine-tune the pore diameter of mesoporous MCM-41 by controlling the pH and TMA fraction, which is a promising approach in pore engineering and molecular sieving with adjustable pore size, and may find wide application in shape-selective catalysis in fine chemicals, bioseparation, and adsorption. pH may be used to control the nickel cluster anchoring (and reduction degree), and this makes it possible to design highly dispersed, stable metallic clusters of controllable size for specific catalytic reactions, such as CO methanation.

Acknowledgment. We are grateful to the DOE, Office of Basic Energy Sciences, for financial support. We also thank NSLS Brookhaven National Laboratory for beam time.

References and Notes

(1) Beck, J. S.; Vartuli, J. C.; Roth, W. J.; Leonowicz, M. E.; Kresge, C. T.; Schmitt, K. D.; Chu, C. T. W.; Olson, D. H.; Sheppard, E. W.; McCullen, S. B.; Higgins, J. B.; Schlenker, J. L. *J. Am. Chem. Soc.* **1992**, *114*, 10834.

(2) Kresge, C. T.; Leonowicz, M. E.; Roth, W. J.; Vartuli, J. C.; Beck, J. S. *Nature* **1992**, *359*, 710.

(3) Ortlam, A.; Rathousky, J.; SchulzEkloff, G.; Zukal, A. *Microporous Mater.* **1996**, *6*, 171.

(4) Kruk, M.; Jaroniec, M.; Sayari, A. *Langmuir* **1997**, *13*, 6267.

(5) Edler, K. J.; Reynolds, P. A.; White, J. W.; Cookson, D. *J. Chem. Soc., Faraday Trans.* **1997**, *93*, 199.

(6) Ravikovitch, P. I.; Wei, D.; Chueh, W. T.; Haller, G. L.; Neimark, A. V. *J. Phys. Chem. B* **1997**, *101*, 3671.

(7) Lukens, W. W.; Schmidt-Winkel, P.; Zhao, D. Y.; Feng, J. L.; Stucky, G. D. *Langmuir* **1999**, *15*, 5403.

(8) Lim, M. H.; Stein, A. *Chem. Mater.* **1999**, *11*, 3285.

(9) Kalipcilar, H.; Culfaz, A. *Cryst. Res. Technol.* **2000**, *35*, 933.

(10) Lim, S.; Ciuparu, D.; Pak, C.; Dobek, F.; Chen, Y.; Harding, D.; Pfefferle, L.; Haller, G. *J. Phys. Chem. B* **2003**, *107*, 11048.

(11) Yang, Y. H.; Lim, S.; Wang, C.; Harding, D.; Haller, G. *Microporous Mesoporous Mater.* **2004**, *67*, 245.

(12) Amama, P. B.; Lim, S.; Ciuparu, D.; Yang, Y. H.; Pfefferle, L.; Haller, G. L. *J. Phys. Chem. B* **2005**, *109*, 2645.

(13) Tanev, P. T.; Chibwe, M.; Pinnavaia, T. J. *Nature* **1994**, *368*, 321.

(14) Zhao, D. Y.; Goldfarb, D. *J. Chem. Soc., Chem. Commun.* **1995**, 875.

(15) Reddy, K. M.; Moudrakovski, I.; Sayari, A. *J. Chem. Soc., Chem. Commun.* **1994**, 1059.

(16) Sayari, A.; Moudrakovski, I.; Danumah, C.; Ratcliffe, C. I.; Ripmeester, J. A.; Preston, K. F. *J. Phys. Chem.* **1995**, *99*, 16373.

(17) Yuan, Z. Y.; Liu, S. Q.; Chen, T. H.; Wang, J. Z.; Li, H. X. *J. Chem. Soc., Chem. Commun.* **1995**, 973.

(18) Cheng, C. F.; Park, D. H.; Klinowski, J. *J. Chem. Soc., Faraday Trans.* **1997**, *93*, 193.

(19) Ryoo, R.; Kim, J. M. *J. Chem. Soc., Chem. Commun.* **1995**, 711.

(20) Lindlar, B.; Kogelbauer, A.; Prins, R. *Microporous Mesoporous Mater.* **2000**, *38*, 167.

(21) Wang, A. J.; Kabe, T. *Chem. Commun.* **1999**, 2067.

(22) Lim, S. Y., Yang, Y. H., Ciuparu, D., Wang, C., Chen, Y., Pfefferle, L., Haller, G. L. *Top. Catal.* **2005**, *34*, 31.

(23) Barrett, E. P.; Joyner, L. G.; Halenda, P. P. *J. Am. Chem. Soc.* **1951**, *73*, 373.

(24) Stern, E. A.; Newville, M.; Ravel, B.; Yacoby, Y.; Haskel, D. *Physica B* **1995**, *209*, 117.

(25) Ankudinov, A. L.; Ravel, B.; Rehr, J. J.; Conradson, S. D. *Phys. Rev. B* **1998**, *58*, 7565.

(26) Pak, C.; Haller, G. L. *Microporous Mesoporous Mater.* **2001**, *48*, 165.

(27) Monnier, A.; Schuth, F.; Huo, Q.; Kumar, D.; Margolese, D.; Maxwell, R. S.; Stucky, G. D.; Krishnamurty, M.; Petroff, P.; Firouzi, A.; Janicke, M.; Chmelka, B. F. *Science* **1993**, *261*, 1299.

(28) Yang, Y. H., Lim, S. Y., Du, G. A., Chen, Y., Ciuparu, D., Haller, G. L. *J. Phys. Chem. B* **2005**, *109*, 13237.